Bioorganic Chemistry 101 (2020) 103964

Contents lists available at ScienceDirect

Bioorganic Chemistry

journal homepage: www.elsevier.com/locate/bioorg

3-Arylcoumarins as highly potent and selective monoamine oxidase B inhibitors: Which chemical features matter?

Marco Mellado[a], Jaime Mella[b,*], César González[c], Dolores Viña[d,e], Eugenio Uriarte[f,g], Maria J. Matos[f,h,*]

[a] Facultad de Ciencias, Instituto de Química, Pontificia Universidad Católica de Valparaíso, Av. Universidad #330, Curauma, Valparaíso, Chile
[b] Instituto de Química y Bioquímica, Facultad de Ciencias, Universidad de Valparaíso, Av. Gran Bretaña 1111, Valparaíso, Chile
[c] Departamento de Química, Universidad Técnico Federico Santa María, Av. España 1680, Valparaíso, Chile
[d] Chronic Diseases Pharmacology Group, Center for Research in Molecular Medicine and Chronic Diseases (CIMUS), Universidade de Santiago de Compostela, 15782 Santiago de Compostela, Spain
[e] Departamento de Farmacología, Farmacia y Tecnología Farmacéutica, Universidade de Santiago de Compostela, 15782 Santiago de Compostela, Spain
[f] Departamento de Química Orgánica, Facultade de Farmacia, Universidade Santiago de Compostela, 15782 Santiago de Compostela, Spain
[g] Instituto de Ciencias Químicas Aplicadas, Universidad Autónoma de Chile, 7500912 Santiago, Chile
[h] CIQUP/Department of Chemistry and Biochemistry, Faculty of Sciences, University of Porto, 4169-007 Porto, Portugal

ARTICLE INFO

Keywords:
3-Arylcoumarins
Monoamine oxidase B inhibitors
3D-QSAR models
Molecular docking
Drug design

ABSTRACT

Monoamine oxidase B inhibitory activity is closely regulated by the interaction of the small molecules with the enzyme. It is therefore desirable to use theoretical approaches to design rational methods to develop new molecules to modulate specific interactions with the protein. Here, we report such methods, and we illustrate their successful implementation by studying six synthetized 3-arylcoumarins (**71**–**76**) based on them. Monoamine oxidase B inhibition is essential to maintain the balance of dopamine, and one of its major functions is to combat dopamine degradation, a phenomenon linked to Parkinson's disease. In this work, we study small-molecule inhibitors based on the 3-arylcoumarin scaffold and their monoamine oxidase B selective inhibition. We show that 3D-QSAR models, in particular CoMFA and CoMSIA, and molecular docking approaches, enhance the probability to find new interesting inhibitors, avoiding very costly and time-consuming synthesis and biological evaluations.

1. Introduction

Parkinson's disease (PD) is the second most common neurodegenerative disease, affecting worldwide ~ 41 people per 100,000 among those under 50, and rising to > 1900 people per 100,000 among those over 80 years [1]. Although PD's pathogenesis is not fully understood, it is known to start with the loss of dopaminergic neurons of the substance nigra pars compacta [1]. There is also evidence that several genetic and environmental factors may be involved, causing oxidative stress, inflammatory processes, mitochondrial injury, abnormal α-synuclein deposition and cell apoptosis. At the moment, the treatment of this disease is only symptomatic. Some therapeutic options are monoamine oxidase B (MAO-B) inhibitors [2], acetylcholinesterase (AChE) inhibitors [3], catechol-*O*-methyltransferase (COMT) inhibitors [4], dopamine agonists or amantadine [5], which is used in early stages or to relieve dyskinesia caused by levodopa-carbidopa [6]. To date, a disease-modifying therapy has not been developed. Therefore, it is urgent to find new chemical entities to control the evolution of the disease [7].

The coumarin framework is a privileged scaffold in Medicinal Chemistry [8,9] Several groups have been studying synthetic pathways to obtain molecules containing this skeleton, as well as their biological properties against different targets. Because of its chemical simplicity, and special aromaticity/planarity, the coumarin is been used as core for more complex chemical structures for multifactorial diseases, as Parkinson's disease [10–12]. Coumarins, specially substituted at three, six or seven positions attracted special interest for their inhibition of enzymes involved on neurodegenerative diseases [13–19].

For more than ten years, our research group has been focused on the synthesis and biological evaluation of differently substituted coumarins as potential MAO-B inhibitors [20–23]. Our research has been supported by several theoretical tools (mainly docking studies) that allowed us accelerating the process to obtain potent and selective MAO-B

* Corresponding authors at: Departamento de Química Orgánica, Facultade de Farmacia, Universidade Santiago de Compostela, 15782 Santiago de Compostela, Spain (M. Matos).
E-mail addresses: jaime.mella@uv.cl (J. Mella), mariajoao.correiapinto@usc.es, maria.matos@fc.up.pt (M.J. Matos).

https://doi.org/10.1016/j.bioorg.2020.103964
Received 26 March 2020; Received in revised form 2 May 2020; Accepted 20 May 2020
Available online 26 May 2020
0045-2068/

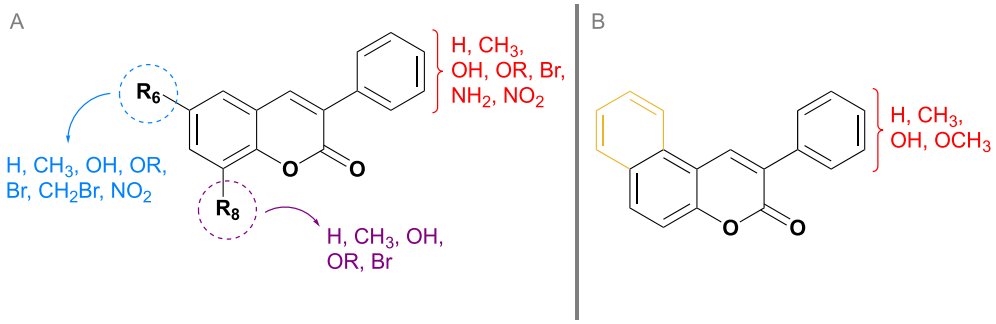

Fig. 1. Structural characteristics of the molecules included in the database. **(A)** 3-arylcoumarins and **(B)** 3-arylbenzo[*f*]coumarin.

inhibitors [24]. Different structural features have been considered and explored. From all the studied families, 3-arylcoumarins proved to be the most promising molecules, with inhibitory activities in the micro, nano and even picomolar ranges. In parallel, other targets related to neurodegenerative diseases have also been considered and studied, in order to evaluate the multitarget profile of this interesting scaffold.

In the current work, 3D quantitative structure–activity relationship models (3D-QSAR) models, in particular Comparative Molecular Field Analysis (CoMFA) and Comparative Molecular Similarity Indices Analysis (CoMSIA), and molecular docking calculations, were used to systematize the structural key points to design potent and selective MAO-B inhibitors, taking as starting point an internal database of seventy compounds previously synthetized and studied as MAO inhibitors by our research group.

2. Results and discussion

2.1. 3D-QSAR: CoMFA and CoMSIA

2.1.1. Statistical results

A database of seventy compounds, generally illustrated in Fig. 1, and detailed in the Supporting Information, was constructed taking into account previous results from our research group on the synthesis and evaluation against MAO enzymes. In particular, we focused our attention on MAO-B selective inhibitors, as most of our compounds present a very high selectivity index towards this isoform.

Using this structural information, 3D-QSAR CoMFA and CoMSIA models were performed. Before analyzing the contour maps, statistical results were analyzed, and the new models were validated. Table S1 shows the statistical results of all CoMFA and CoMSIA models generated from all possible field combinations (steric, electrostatic, hydrophobic or hydrophilic, hydrogen bond donor and hydrogen bond acceptor). For each model, the value of the cross-validation coefficient (q^2) was determined. This parameter should be higher than 0.5 for a model to be considered valid. The value of q^2 indicates how good the model is for predicting the biological activity of the molecules that are the training set of the model. In the case of CoMFA –the model that considered both the steric and electrostatic contributions (CoMFA-SE)– it gave the best q^2value (0.924). In addition, the model presented a low value in the number of components (N = 3) and the high value for the regression coefficient (r_{ncv}^2 = 0.987).

On the other hand, most CoMSIA models presented high values for q^2. The models CoMSIA-E, D, A, ED, EA, EDA, and DA have a q^2 value lower than 0.5. From the rest, only one model has q^2 value higher than 0.9 (CoMSIA-S). However, this model has a high number of components (N = 5). The models with the best q^2 values were CoMSIA-S, SEH, SH, SD and SA. The CoMSIA-DA model showed the lowest value for q^2 (-0.068), so models that consider the H-bond donor and acceptor contributions were discarded. On the other hand, CoMSIA-S, SH, SD and SDA models presented a very high number of components (N ≥ 10), so they were also discarded. Therefore, the best model in terms of high q^2 value, low number of components, and balance between field contributions, was the CoMSIA-SHE model. From now on, the best models –CoMFA-SE and CoMSIA-SEH– will be mentioned as CoMFA and CoMSIA models, to simplify.

In order to validate the predictive capacity of both models, a series of parameters were determined (Table S2). The value of r^2 is a measure of the external predictive capability of the model. A value of $r^2 > 0.6$ is considered as acceptable. High r^2 values indicate that the model has a good ability to predict the activity of molecules out of the training set. As can be observed in Table S2, the models presented good r^2 values (0.947 and 0.896 for CoMFA and CoMSIA, respectively). This information is aligned with the predictions for the test set (Fig. 2). According to Golbraikh and Tropsha, high values of q^2 and r^2 (conditions 1 and 2, Table S2) are necessary but not sufficient conditions for the model validation [25]. For a QSAR model to have a reliable predictive capability, the line of experimental *versus* predicted activities should be as close as possible to the line $y = x$. This is observed with the fulfillment of conditions (3a or 3b), (4a or 4b) and (5a or 5b), listed in Table S2. Condition 7, known as r_m^2 metrics, is a quantitative measure to determine the agreement between the observed and predicted activities for the test set. CoMFA and CoMSIA models reported here fulfilled all the conditions for internal and external validation. In addition, the calculation of several external validation descriptors (conditions 7 to 12) was performed [26,27,28]. In all cases, our models passed the validation tests. The only value that is slightly below the standard is Q_{F3}^2, for CoMSIA (Table S2).

For both models, there is a good distribution along the ideal line $y = x$. The external validation of the models evaluates how close this line is to the ideal line. Furthermore, the Y-randomization test (Table S3) was applied to assess the robustness of both models [29]. The dependent variable (biological activity) was randomly shuffled and a new QSAR model was developed using the original independent variable matrix. If after multiple randomizations the new values of q^2 and r_{ncv}^2 are negative or below the limit of acceptability ($q^2 < 0.5$, $r_{ncv}^2 < 0.6$), it is corroborated that the results obtained in the formulation of the final models are not by chance. In our case, the new QSAR models (after several repetitions) have low q^2 and r_{ncv}^2 values (Table S3). Only in randomizations 2 and 3, high values for r_{ncv}^2 were obtained. However, the values of q^2 were always negative.

The chemical structures of the dataset, values of experimental activity, predicted activity and residual values for the CoMFA and CoMSIA models, are shown in Tables S4 and S5. Analyses were performed on seventy molecules presenting high structural diversity on the 3-arylcoumarin scaffold (Table S4). Fifty-one compounds were used as a training set (73%) and nineteen as a test set (27%). For both models, the compounds used as training and test sets were the same. The CoMFA model presented a total of thirty-four compounds with negative deviations in the predicted activity values and thirty-six compounds with positive deviations. The largest deviations for biological activity were observed for the 3-(2′-bromophenyl)-6-methylcoumarin (**10**), 6-bromo-8-hydroxy- 3-(4′-hydroxyphenyl)coumarin (**25**) and 3-

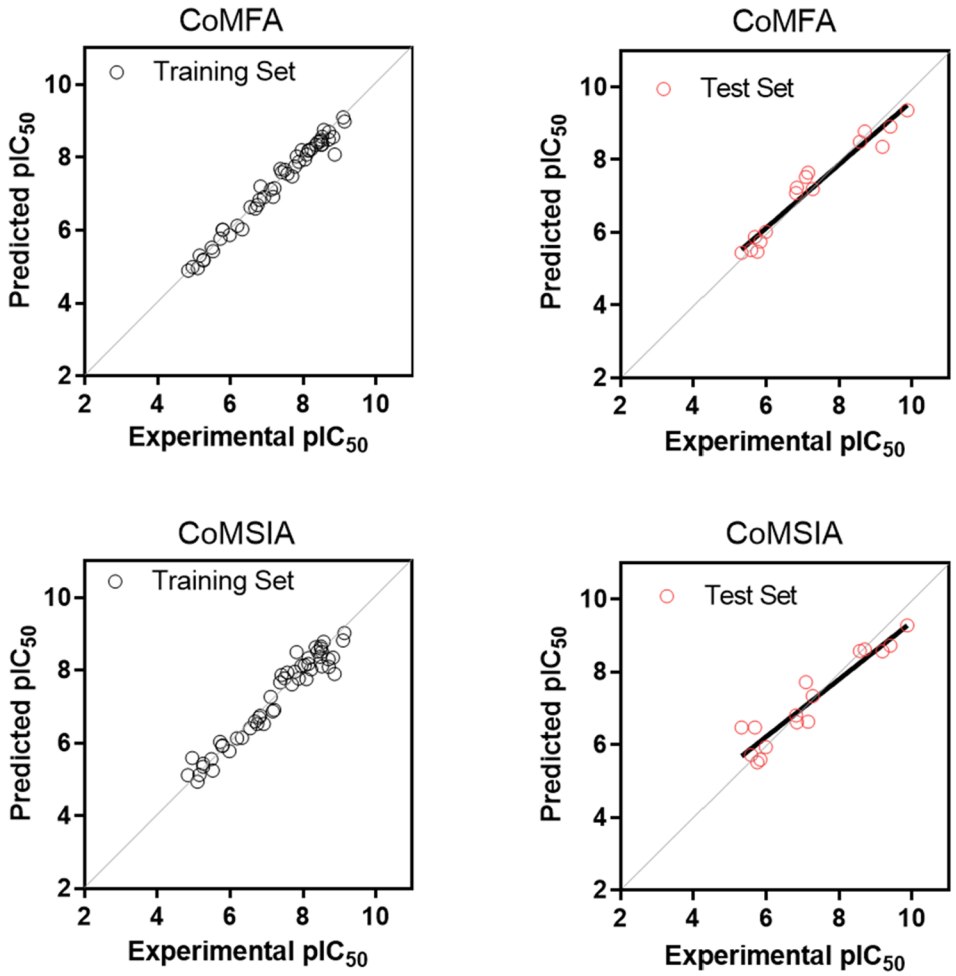

Fig. 2. Plots of experimental *versus* predicted pIC_{50} values for the training and test set compounds. On the right, in black, predictions for the training set. On the left, in red, predictions for the test set. For the test set, in each case, the regression line for r^2 is shown in dark black. (For interpretation of the references to color in this figure legend, the reader is referred to the web version of this article.)

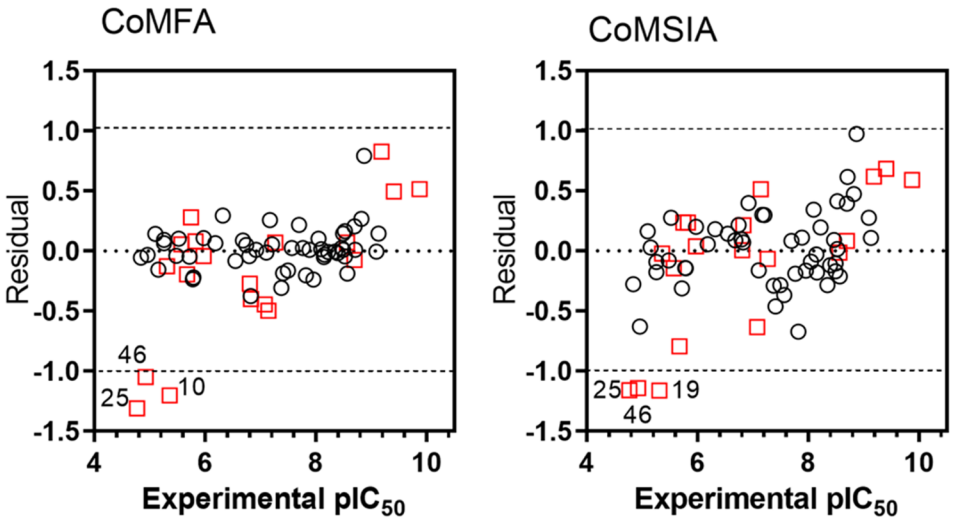

Fig. 3. Graphs of residual (experimental pIC_{50} - predicted pIC_{50}) distribution *versus* biological activity for CoMFA and CoMSIA models. In each case, the compounds that experienced a deviation greater than one logarithmic unit in the predicted value of activity by the equation are indicated (outlier compounds; residual > 1.0). Color code: black spheres, training set; red squares, test set. (For interpretation of the references to color in this figure legend, the reader is referred to the web version of this article.)

phenylcoumarin (**46**) (negative deviations). These compounds presented residual values, higher than one logarithmic unit (Fig. 3). Therefore, they correspond to outliers. In the case of the CoMSIA models, thirty-three compounds presented negative deviations in the predicted values of activity, while thirty-seven compounds presented positive deviations. In the CoMSIA model, the outlier compounds are the 8-bromo-6-methyl-3-(3′,4′,5′-trimethoxyphenyl)coumarin (**19**), 6-bromo-8-hydroxy- 3-(4′-hydroxyphenyl)coumarin (**25**) and 3-phenylcoumarin (**46**) (negative deviations, higher than 1 log unit). Therefore, in terms of error, both models are similar. On the other hand, the graphs of the distribution of residuals *versus* biological activity (Fig. 3) showed an adequate balance in terms of distribution of

residuals across the entire range of biological activity. The largest deviations in both cases were observed in low activity ranges (pIC_{50} < 6.0). The greatest dispersion of residuals occurred for CoMSIA.

2.2. Applicability domain

The applicability domain is a theoretical region in chemical space encompassing both the model descriptors and modeled response. It allows estimating the uncertainty in the prediction of a compound based on how similar it is to the training compounds employed in the model. In this work, we used the method developed by Roy *et al.* for determining the applicability domain, which is based on the basic theory of the standardization approach [30]. For both CoMFA and CoMSIA, all the compounds (training and test set) were within the applicability domain.

2.3. Contour maps analysis

QSAR studies allow systematizing the information on the structure–activity relationship (SAR) of the series of computations in order to design new molecules. QSAR studies can predict the activity of the proposed molecules. On the other hand, the error involved in performing a qualitative SAR analysis is minimized. Unlike a 2D-QSAR, the results of a 3D-QSAR can be represented as contour maps around the studied molecules. The analysis of the different colored polyhedrons around a molecule (i.e. the most active compound in the series) allows understanding the main characteristics that are favorable or unfavorable for the affinity or biological activity. This is the main goal of the current theoretical approaches.

2.4. Steric contour maps

The steric contour maps from the CoMFA (Fig. 4A and B) and CoMSIA (Fig. 5A and B) analysis are consistent with each other. The best MAO-B inhibitor obtained from the training set [3-(3′-bromo-4′-methoxyphenyl)-6-methylcoumarin, **7**] and the least good MAO-B inhibitor obtained from the training set [6-(cyclopentyloxy)-3-(*p*-tolyl) coumarin, **49**] where selected for this study. Green polyhedrons can be observed around the aromatic ring at position 3 of the coumarin scaffold (Fig. 4A and 5A for compound **7**, and Fig. 4B and 5B for compound **49**). Therefore, bulky substitutions at *meta* and *para* positions (Fig. 1) are favorable in this region, as observed by the green polyhedrons in Fig. 4A and 5A, for compound **7**. This information is corroborated by the trend showed by several 3-arylcoumarins presenting high values of MAO-B inhibitory activity (i.e. MAO-B pIC_{50} values higher than 8.0 for compounds **3**, **7**, **9**, **11**, **14**, **15**, **17**, **18**, **24**, **26**, **28**, **29**, **31**, **35**, **39**, **40**, **45**, **48**, **53**, **54**, **57–59** and **61**, Table S5). The versatility of these substituents, as observed in Table S4, can be high. Methyl, methoxy, hydroxyl or amine groups, as well as bromine atoms, are allowed in both positions. Combinations of substituents in both *meta* and *para* positions, as 3-(3′-bromo-4′-methoxyphenyl)-6-methylcoumarin (**7**), are an excellent option to optimize the potential of these molecules (MAO-B pIC_{50} of 9.133). In the same range of MAO-B inhibitory activity, 3-(3′-bromophenyl)-6-methylcoumarin (**14**) and 3-(4′-bromophenyl)-6-methylcoumarin (**15**) proved that mono-substitutions are also a great choice (MAO-B pIC_{50} of 9.873 and 9.409, respectively). In both cases, a halogen atom at *meta* or *para* positions seems to be recommendable. For compounds that do not present substituents other than hydrogen atoms in these positions, the activity decreases. This can be seen, for example, for the 8-ethoxy-3-phenylcoumarin (**20**) and 3-phenylcoumarin (**46**), with MAO-B pIC_{50} values lower than 6.0 (Table S5).

From the steric CoMSIA map, it is concluded that the presence of a bulky substitution at position 6 of the coumarin scaffold can lead to decrease the MAO-B inhibitory activity (yellow polyhedron in Fig. 5A and B, for compounds **7** and **49**, respectively). For example, the 6-methoxy-3-(*p*-tolyl)coumarin (**35**) presented a MAO-B pIC_{50} of 8.824. However, by changing the methoxy group by a larger side chain, as the 6-(2-oxopropoxy)-3-(*p*-tolyl)coumarin (**43**), the MAO-B pIC_{50} decreased to 5.258. Likewise, by changing the same substituent for an even bulkier one such as *O*-cyclopentyl, the MAO-B pIC_{50} decreased to 4.840 (compound **49**). A similar trend can be observed for the naphthylcoumarin derivatives. Compounds **60–70** (with this extra fused ring) *versus* i.e. compounds **2–4**, **6–9** (6-methylcoumarins), presented on average 1 logarithmic unit less of MAO-B inhibitory activity (Table S5).

2.5. Electrostatic contour maps

The presence of a red polyhedron around the *meta* and *para*

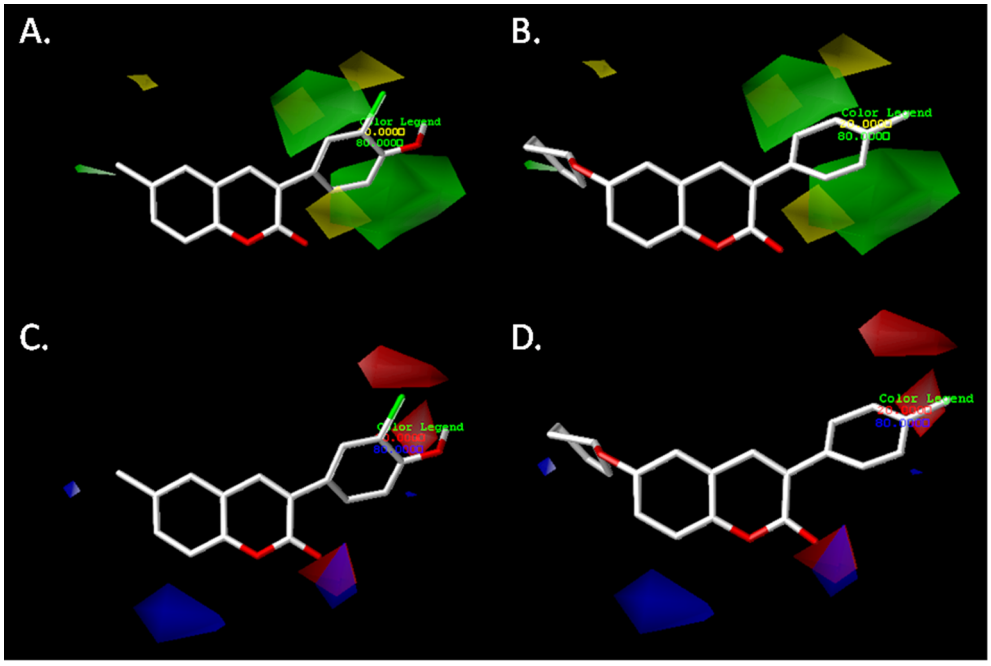

Fig. 4. CoMFA steric (**A** and **B**) and electrostatic (**C** and **D**) contour maps around the most active compound obtained from the training set (**7**, at the left) and the less active compound obtained from the training set (**49**, at the right). Color code: green, bulky groups are favorable for activity; yellow, small groups are favorable for activity; red, negative charge is favorable for activity; blue, positive charge is favorable for activity. (For interpretation of the references to color in this figure legend, the reader is referred to the web version of this article.)

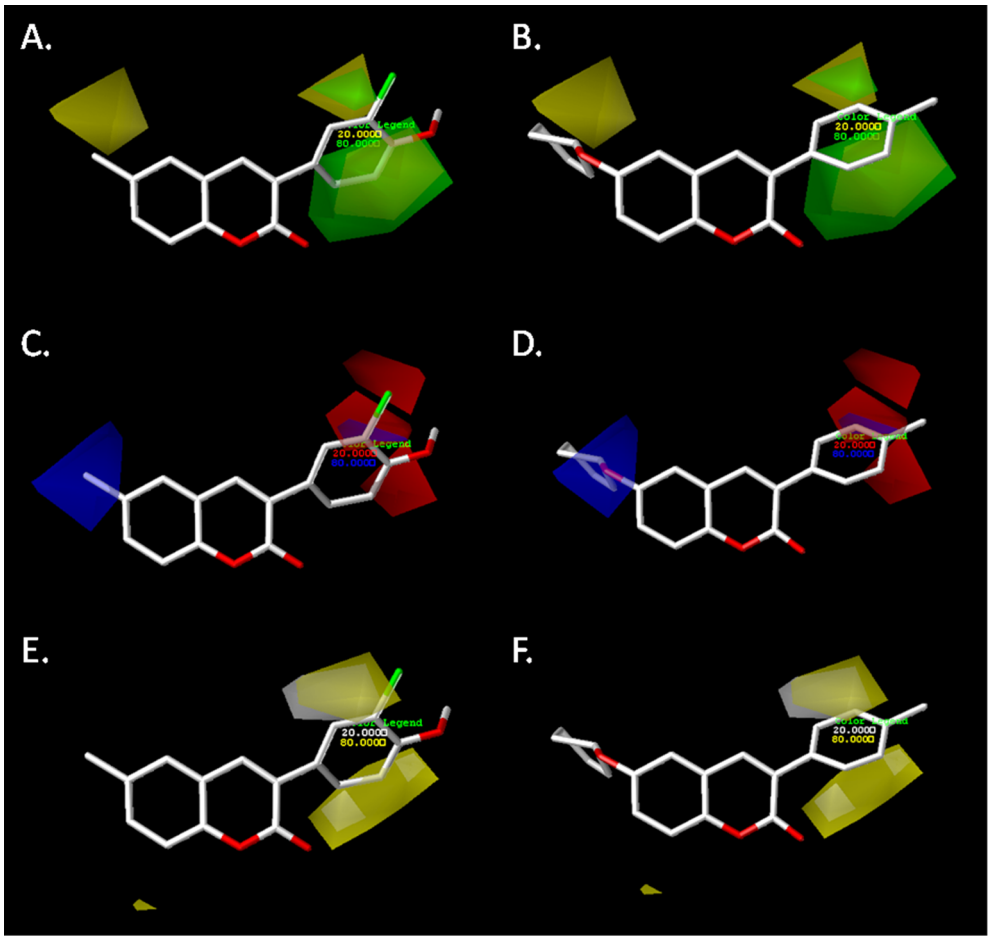

Fig. 5. CoMSIA steric (**A** and **B**), electrostatic (**C** and **D**) and hydrophobic (**E** and **F**) contour maps around the most active compound obtained from the training set (**7**, at the left) and the less active compound obtained from the training set (**49**, at the right). Color code: green, bulky groups are favorable for activity; yellow, small groups are favorable for activity; red, negative charge is favorable for activity; blue, positive charge is favorable for activity. For the hydrophobic contour map: yellow, hydrophobic groups are favorable for the activity; grey, hydrophilic groups are favorable for the activity. (For interpretation of the references to color in this figure legend, the reader is referred to the web version of this article.)

positions of the aromatic ring attached at position 3 of the coumarin scaffold means that electron-rich groups such as halogens, hydroxyl, *O*-alkyl and nitro are favorable for the biological activity (i.e. compounds **3**, **7**, **9**, **11**, **14**, **15**, **24**, **26**, **28**, **31**, **39**, **40**, **45** and **57**–**59**, Tables S4 and S5).

The CoMSIA electrostatic contour maps show that an electropositive surface at position 6 of the coumarin scaffold increases activity (blue polyhedron in Fig. 5C and D, for compounds **7** and **49**, respectively). This is seen for the 3-(4′-methoxyphenyl)-6-nitrocoumarin (**59**), which presents a nitro group attached to this position (MAO-B pIC_{50} of 8.523). The positive nitrogen from the nitro group is responsible for the blue polyhedron. When comparing this compound with other derivatives that present substituents that do not have electropositive characteristics, the activity decreases. For example, the 3-(4′-methoxyphenyl)-6-methylcoumarin (**2**) presents a methyl substituent at position 6 and its MAO-B pIC_{50} is 7.886 (Table S5). The 3-(4′-methoxyphenyl)coumarin (**56**) presents a hydrogen substituent at position 6 and its MAO-B pIC_{50} is 5.788 (Table S5).

Finally, the CoMFA analysis shows a red polyhedron on the oxygen of the carbonyl group (Fig. 4C and D, for both compounds **7** and **49**, respectively). This means that this functional group is essential for the MAO-B inhibitory activity, which is evidenced by the activity displayed by all the coumarins presented in this study (Table S5).

2.6. Hydrophobic contour map

CoMSIA hydrophobic contour maps (Fig. 5E and F, for compounds **7** and **49**, respectively) show a grey polyhedron near the *ortho* position of the aromatic ring at position 3 of the coumarin scaffold, indicating that MAO-B inhibitory activity increases with the presence of a hydrophilic substitute (i.e. hydroxyl or amine groups). Indeed, when comparing the activities of the compounds presenting a bromine, hydroxyl and amine substituent in the mentioned position, the order of MAO-B inhibitory activity is OH > NH_2 > Br (i.e. 3-aryl-6-methylcoumarins with 3-*ortho*-substitutions **13**, **52** and **10**, respectively).

Additionally, Fig. 5E and F shows the presence of a yellow polyhedron around the 3-aryl substituent. This indicates that hydrophobic substitutes at these positions increase MAO-B inhibitory activity. For example, this is evident for the 3-(3′-bromo-4′-methoxyphenyl)-6-methylcoumarin (**7**), 3-(3′-bromophenyl)- 6-methylcoumarin (**14**), 3-(4′-bromo-3′-methoxyphenyl)-6-methylcoumarin (**31**), 3-(3′-bromophenyl)-6-methoxycoumarin (**39**), 3-(3′-bromophenyl)-6-hydroxycoumarin (**40**) and 2-(3-(3′-bromophenyl)coumarin-6-yl)oxy)acetyl chloride (**48**) which present substitutions with the previously mentioned characteristics and present MAO-B pIC_{50} values higher than 8.0 (Table S5).

2.7. Molecular docking

The docking analysis was carried out using the Autodock Vina program and the human MAO-B crystalline structure (PDB ID: 1GOS) [31]. These calculations showed that the 3-(3′-bromophenyl)-6-methylcoumarin (**14**, the most active compound from the dataset) presents affinity energy of −7.1 kcal/mol, while the energy for R-(-)-deprenyl was −6.6 kcal/mol. These results are consistent with the reported inhibitory activity for both compounds (MAO-B pIC_{50} = 9.873 and 7.708, respectively). The visualization of the results was performed with PyMOL and Ligplot+ (Fig. 6A-C).

Fig. 6A shows the general 3D visualization of MAO-B with the best pose of the 3-(3′-bromophenyl)-6-methylcoumarin (**14**) within the

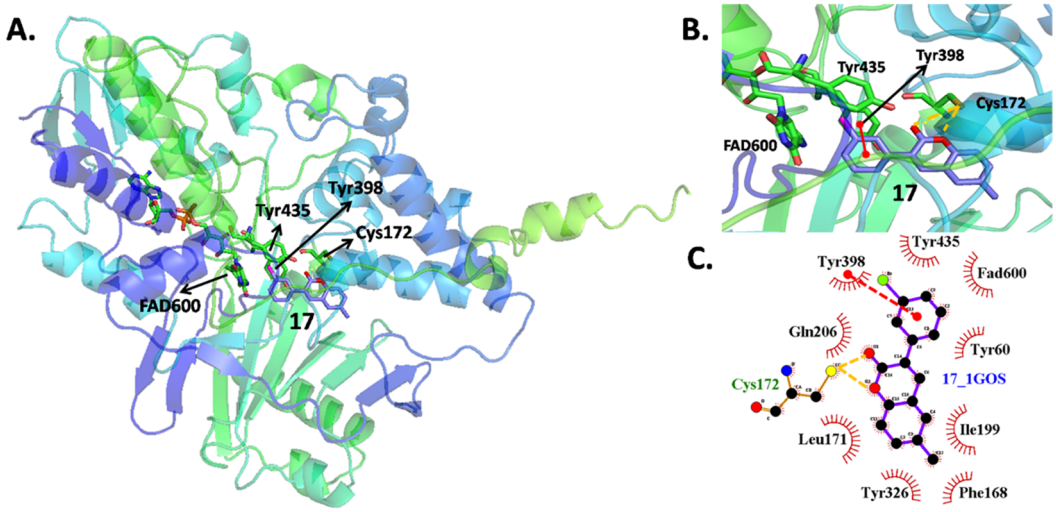

Fig. 6. Molecular Docking results. **(A)** 3D overview of 3-(3′-bromophenyl)-6-methylcoumarin (**14**) within the active site of MAO-B. **(B)** MAO-B inhibition site and key amino acid residues around compound **14**. **(C)** Details of polar and van der Waals interactions established between the MAO-B active site and compound **14**.

active site, highlighting FAD600, Tyr435, Tyr398 and Cys172. Fig. 6B shows an expansion of the active site of MAO-B, where the residue of Cys172 is close to the oxygen atoms of the coumarin scaffold, favoring the formation of a hydrogen bond. This interaction is crucial for the MAO-B inhibition. Fig. 6C shows that the aromatic ring of the 3-arylcoumarin is oriented towards the Gln206, Tyr435, Tyr60 and FAD residues of the MAO-B active site. Comparing this with the 3D-QSAR (Figs. 4 and 5), it is confirmed that the presence of electron-rich substituents at *meta* and *para* positions of the aromatic ring of the 3-arylcoumarins increases the MAO-B inhibitory activity. This may be due to the formation of polar and hydrogen-bond interactions with Tyr60, FAD600 and Tyr435 residues. The last one being one of the responsible for ligand polarization and subsequent reduction of FAD [32].

The residues of Ile199 and Tyr60 are located near position 4 of the coumarin core (Fig. 6C). Compared to the CoMSIA analysis (Fig. 5), the hydrophobic contour map indicates that a substituent of hydrophilic characteristics would increase the MAO-B inhibitory activity. This is consistent with a potential hydrogen bond or dipole interaction with Tyr60 (i.e. in the case of a hydroxyl group).

Ile199, Phe168 and Tyr326 residues are located near position 6 of the coumarin scaffold, which show van der Waals interactions with compound **14** (Fig. 6C). According to 3D-QSAR analysis, a hydrophilic substitute (i.e. a hydroxyl group) increases the MAO-B inhibitory activity. This is consistent with the polar interactions that may be formed with Tyr326. In contrast, an electron-rich substitute generates a decay on the MAO-B inhibitory activity, which could be related to the high electron density of the Tyr326 ring.

Finally, Leu171 and Tyr326 residues are located close to the position 8 of the coumarin nucleus. Comparing with the results obtained by the CoMFA and CoMSIA electrostatic contour maps analyses (Fig. 4C and D, and 5C and D), an electron-rich substituent decreases the MAO-B inhibitory activity. This is consistent with the presence of the Tyr326 residue, which presents a high electron density.

2.8. Summary of the principal results based on the theoretical models

Important structural information has been extracted from the theoretical studies and the new compounds were synthetized based on that. Fig. 7 summarizes of the main structure–activity relationships obtained analyzing the different approaches used in the current study.

Based on the results obtained with both CoMFA and CoMSIA models, and Docking calculations, as more of these requirements are concomitantly fulfilled, a more active compound may be obtained. The simultaneous completion of the three characteristics for the aryl fragment of the coumarin core (bulky and hydrophilic substituents in *ortho* position, electron-rich substituents in *para* position, and lipophilic, electron-rich and bulky substituents in *meta* position) would provide a more active compound than if only one or two substitutions were considered.

2.9. Synthesis and biological evaluation of new compounds

To validate the models experimentally, after analyzing the theoretical results, and to obtain new derivatives based on the information from these models, we carried out the synthesis of 6 new derivatives (Scheme 1 and Table 1, compounds **71–76**) [33]. The compounds were synthesized based on information from the maps, which suggested the presence of lipophilic, bulky and electron-rich groups in the phenyl ring at position 3. Ethoxy, methoxy, methyl and hydroxyl groups and bromine atoms were selected as the best substituents. They were attached strategically to the best positions predicted by the models. The experimental and theoretical results obtained by CoMFA and CoMSIA models are presented in Table 1.

The synthesis of the new compounds was carried out via a traditional Perkin reaction of different *ortho*-hydroxybenzaldehydes with the corresponding arylacetic acids, using *N,N'*-dicyclohexylcarbodiimide (DCC) as dehydrating agent, in the presence of dimethylsulfoxide (DMSO), at 110 °C, for 24 h. This reaction afforded compounds **72–74**, **76** and the precursors of compounds **71** and **75** (named **9** and **75′**, respectively). Compound **71** was obtained by acidic hydrolysis of the respective methoxy derivative **9**, using hydriodic acid 57% in the presence of acetic acid and acetic anhydride, in reflux, for 3 h. Finally, compound **75** was prepared by brominating the precursor **75′**, in the presence of *N*-bromosuccinimide (NBS), using azobisisobutyronitrile (AIBN) as catalysator, in the presence of carbon tetrachloride (CCl_4), in reflux, for 18 h.

The potential effects of the compounds **71–76** on *h*MAO-B activity were investigated by measuring the production of hydrogen peroxide (H_2O_2) from *p*-tyramine, using an Amplex® Red MAO assay kit and MAO isoform prepared from insect cells (BTI-TN-5B1-4) infected with recombinant baculovirus containing cDNA inserts for *h*MAO-B. The inhibition of *h*MAO activity was evaluated following a general procedure previously described [20]. Experimental results are expressed as IC_{50} values of *h*MAO-B inhibitory activity effects of the tested compounds and are shown in Table 1. All of the compounds in this study resulted to be *h*MAO-B inhibitors in the low micro or low nanomolar ranges.

The best compound within the synthetized series –3-(3′,5′-

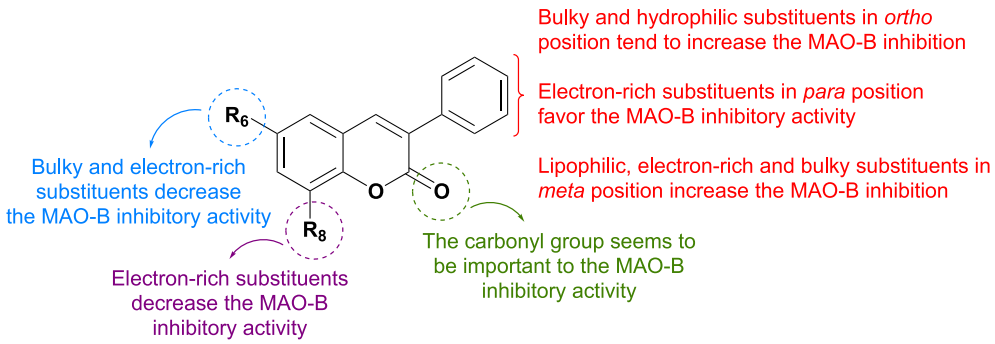

Fig. 7. Summary of the main structure–activity relationships found in this study.

dimethoxyphenyl)-8-methylcoumarin (**72**)– presents a MAO-B pIC_{50} of 8.187, corroborating the structural information obtained by the CoMFA and CoMSIA studies. 3-(5′-Bromo-2′,4′-dimethoxyphenyl)-6-methylcoumarin (**75**) and 8-methoxy-3-(*m*-tolyl)coumarin (**76**) display activities in the same range. One is a 6-methyl derivative, and the other one an 8-methoxy derivative. As mentioned above, both positions are interesting in order to optimize the best lead compound. Also, both methyl and methoxy groups (electron donating groups) prove to be good substituents to increase the potential of the molecules. Regarding the substitution pattern on the aromatic ring in the position 3 of the coumarin scaffold, compound **75** presents a methoxy group at position *ortho*, a position potentially undesirable for the MAO-B inhibitory activity. However, the methoxy group is consider a bulky and is mildly hydrophilic group, therefore may be positive for the activity. In addition, the presence of another methoxy in *para* position and an extra bromine atom in *meta*, seems to balance the risk–benefit of having a substituent in *ortho*. From this short series, it can also be extrapolated that increasing the side chain at position 8 (i.e. 8-ethoxy derivatives **73** and **74**), the activity tends to decrease (MAO-B pIC_{50} of 4.971 and 5.607, respectively).

To validate the potential of the new compounds as selective MAO-B inhibitors, and corroborate the theoretical results previously obtained using the CoMFA and CoMSIA models, their *h*MAO-A inhibitory activities were also evaluated. From the series, only compound **71** proved to inhibit *h*MAO-A isoenzyme (IC_{50} = 6.4 μM). All the other synthetized molecules proved to be inactive at 100 μM, the highest tested concentration. These results are closely aligned with the previous results reported by our group.

Table 1
Experimental MAO-B inhibition values (IC_{50} and pIC_{50}) and predicted activity (pIC_{50} CoMFA and pIC_{50} CoMSIA) for compounds **71–76**.

Compound	IC_{50} MAO-B	pIC_{50} MAO-B	pIC_{50} CoMFA	pIC_{50} CoMSIA
71	4.7 μM	5.327	6.067	5.987
72	6.5 nM	8.187	8.125	8.284
73	10.7 μM	4.971	5.654	5.852
74	2.5 μM	5.607	5.605	5.589
75	132 nM	6.879	6.480	7.254
76	81 nM	7.092	7.413	7.339

Finally, based on the SAR results, there is an adequate balance between the predictions made by the CoMFA and CoMSIA models and the experimental results (Fig. 8). As observed, there is an adequate distribution of values along the $y = x$ line.

3. Conclusion

In this study, we constructed two robust 3D-QSAR models –CoMFA and CoMSIA– based on a series of compounds previously reported by our research group. The molecules present a 3-arylcoumarin scaffold, known for their potent and selective MAO-B inhibitory activity. The best models obtained were validated internal and externally. The obtained values of q^2 were 0.924 and 0.863 for CoMFA and CoMSIA,

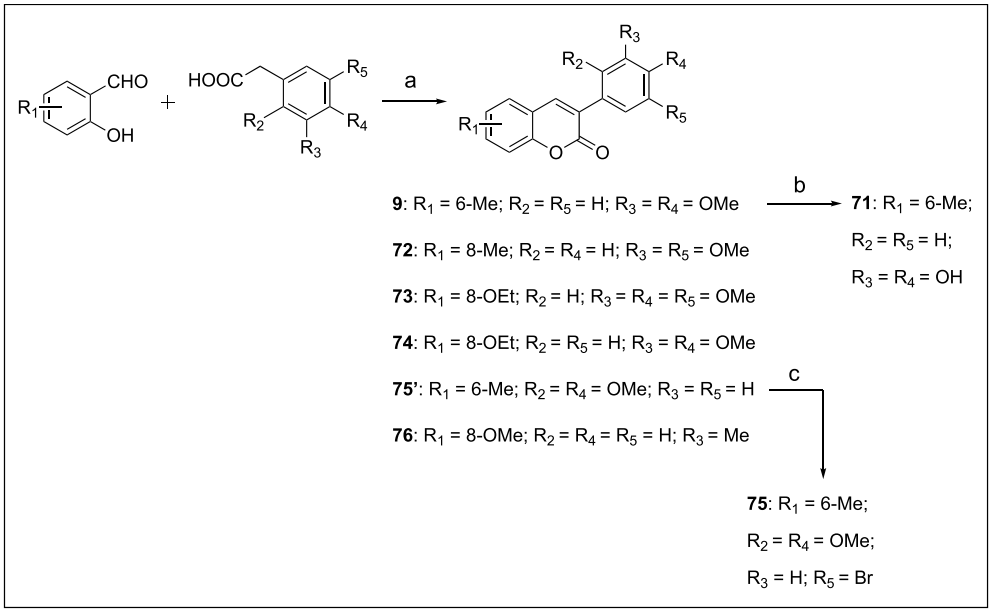

Scheme 1. Reagents and conditions: **(a)** DCC (1.56 equiv), DMSO, 110 °C, 24 h; **(b)** HI, AcOH, Ac_2O, reflux, 3 h; **(c)** NBS (1.2 equiv), AIBN (cat.), CCl_4, reflux, 18 h.

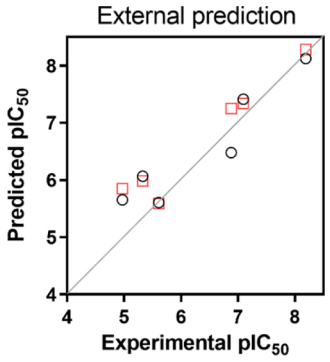

Fig. 8. Values of experimental *versus* predicted MAO-B inhibitory activity for the synthesized compounds (**71–76**). Color code: black spheres, CoMFA predictions; red squares, CoMSIA predictions. (For interpretation of the references to color in this figure legend, the reader is referred to the web version of this article.)

respectively. The r^2 values for the set test were 0.863 and 0.896 for CoMFA and CoMSIA, respectively. Therefore, it can be concluded that both models are reliable and present good external predictive capability. To validate the models experimentally, six new molecules have been synthesized. The most powerful compound [3-(3′,5′-dimethoxyphenyl)-8-methylcoumarin] presented an IC_{50} = 6.5 nM. The predictions for the synthesized compounds followed an adequate distribution along the $y = x$ line. Docking calculations have also been taken into account in the current study. Some important structural features that may conditioning the biological activity can be highlighted analyzing all the theoretical data together. Regarding the aromatic ring at position 3 of the coumarin scaffold, bulky and hydrophilic substituents in *ortho* position tend to increase the MAO-B inhibition. Also, electron-rich substituents in *para* position favor the activity. Finally, lipophilic, electron-rich and bulky substituents in *meta* position increase the inhibitory activity as well. Substitution patterns at position 6 of the coumarin scaffold were also analyzed. Bulky and electron-rich substituents may contribute to decrease the MAO-B inhibitory activity. Finally, at position 8, the presence of electron-rich substituents decreases the MAO-B inhibitory activity. The combination of substituents at both the coumarin core and the aromatic ring at position 3 may be the key for the successful design of new molecules. Based on all this information, it can be concluded that the developed 3D-QSAR models constitute a robust tool for the design of new MAO-B inhibitors presenting the 3-arylcoumarin scaffold.

4. Experimental section

4.1. Chemistry: Synthesis of the new compounds

4.1.1. General information

All reagents were purchased from Sigma-Aldrich and used without further purification. All solvents were commercially available grade. All reactions were carried out under argon atmosphere, unless otherwise mentioned. Reaction mixtures were purified by flash column chromatography using Silica Gel high purity grade (Merck grade 9385 pore size 60 Å, 230–400 mesh particle size). Reaction mixtures were analyzed by analytical thin-layer chromatography (TLC) using plates precoated with silica gel (Merck 60 F254, 0.25 mm). Visualization was accomplished with UV light (254 nm) or potassium permanganate ($KMnO_4$). ^{1}H NMR and ^{13}C NMR spectra were recorded on a Bruker AMX spectrometer at 250 and 75.47 MHz in the stated solvents ($CDCl_3$ or DMSO-d_6) using tetramethylsilane (TMS) as an internal standard. Chemical shifts were reported in parts per million (ppm) on the δ scale from an internal standard (NMR descriptions: s, singlet; d, doublet; dd, double-doublet; t, triplet; q, quadruplet; m, multiplet). Mass spectroscopy was performed using a Hewlett-Packard 5988A spectrometer. This system is an automated service utilizing electron impact (EI) ionization. Elemental analyses were performed using a Perkin-Elmer 240B microanalyser and were within (0.4% of calculated values in all cases. The purity of compounds was assessed by HPLC and was found to be higher than 99%.

4.2. Synthetic methodologies

A solution of *ortho*-hydroxybenzaldehyde (1.0 mmol), the corresponding arylacetic acid (1.25 mmol) and DCC (1.56 mmol), in DMSO (2.0 mL), was heated at 110 °C in an oil bath for 24 h. Ice (20 g). AcOH (3.0 mL) was added and the mixture was stirred at room temperature for 2 h, and then extracted with Et_2O (3 Å~ 25 mL). The combined organic layer was washed with 5% aqueous $NaHCO_3$ solution (50 mL) and H_2O (20 mL) and dried (Na_2SO_4). The solvent was evaporated under vacuum and the residue was purified by flash chromatography (hexane–EtOAc, 9:1) to give the coumarins **9**, **72–74**, **75′** and **76**.

3-(3′,4′-Dimethoxyphenyl)-6-methylcoumarin (9). Yield: 71%; Mp 149–150 °C. ^{1}H NMR ($CDCl_3$) δ: 2.40 (s, 3H, CH_3), 3.92 (s, 3H, OCH_3), 3.94 (s, 3H, OCH_3), 6.92 (d, 1H, H-5′, J = 8.3), 7.21–7.29 (m, 5H, H-5, H-7, H-8, H-2′, H-6′), 7.72 (s, 1H, H-4). ^{13}C NMR ($CDCl_3$) δ: 20.7, 55.8, 55.9, 99.3, 110.8, 111.6, 115.9, 119.4, 121.1, 127.4, 127.5, 132.0, 134.0, 138.7, 148.5, 149.5, 151.3, 160.8. MS *m/z* (%): 297 (28), 296 (M^+, 100). Anal. Elem. Calc. for $C_{18}H_{16}O_4$: C, 72.96; H, 5.44. Found: C, 72.90; H, 5.49.

3-(3′,5′-Dimethoxyphenyl)-8-methylcoumarin (72). Yield 58%. Mp 104–105 °C. ^{1}H NMR ($CDCl_3$) δ: 2.51 (s, 3H, CH_3), 3.85 (s, 6H, 2xOCH_3), 6.52 (t, 1H, H-4′, J = 2.3), 6.87 (d, 2H, H-2′, H-6′, J = 2.3), 7.22 (d, 1H, H-7, J = 7.8), 7.32–7.40 (m, 2H, H-5, H-6), 7.81 (s, 1H, H-4). ^{13}C NMR ($CDCl_3$) δ: 15.4, 55.4, 55.5, 100.8, 106.7, 106.7, 119.2, 124.0, 125.6, 125.9, 127.7, 132.8, 136.7, 140.4, 140.6, 151.8, 160.6. MS *m/z* (%): 297 (37), 296 (M^+, 100). Anal. Elem. Calc. for $C_{18}H_{16}O_4$: C, 72.96; H, 5.44. Found: C, 73.04; H, 5.51.

8-Ethoxy-3-(3′,4′,5′-trimethoxyphenyl)coumarin (73). Yield 40%. Mp 142–143 °C. ^{1}H NMR ($CDCl_3$) δ: 1.58 (t, 3H, CH_3, J = 7.0), 3.94 (s, 3H, OCH_3), 3.96 (s, 3H, OCH_3), 3.99 (s, 3H, OCH_3), 4.25 (q, 2H, CH_2, J = 7.0), 7.0 (s, 2H, H-2′, H-6′), 7.14–7.20 (m, 1H, H-6), 7.24–7.27 (m, 1H, H-7), 7.30–7.32 (m, 1H, H-5), 7.83 (s, 1H, H-4). ^{13}C NMR ($CDCl_3$) δ: 14.8, 56.2, 56.3, 65.0, 105.9, 114.5, 119.2, 120.3, 124.4, 128.2, 130.2, 139.7, 133.8, 146.3, 153.0. MS *m/z* (%): 357 (23), 356 (M^+, 100). Anal. Elem. Calc. for $C_{20}H_{20}O_6$: C, 67.41; H, 5.66. Found: C, 67.42; H, 5.68.

8-Ethoxy-3-(3′,4′-dimethoxyphenyl)coumarin (74). Yield 41%. Mp 138–139 °C. ^{1}H NMR ($CDCl_3$) δ: 1.53 (t, 3H, CH_3, J = 7.0), 3.90 (s, 3H, OCH_3), 3.95 (s, 3H, OCH_3), 4.21 (q, 2H, CH_2, J = 7.0), 6.94 (d, 1H, H-7, J = 8.2), 7.02–7.09 (m, 2H, H-2′, H-6′), 7.20 (d, 1H, H-5′, J = 7.9), 7.28–7.33 (m, 2H, H-5, H-6), 7.77 (s, 1H, H-4). ^{13}C NMR ($CDCl_3$) δ: 14.5, 55.7, 64.6, 110.7, 111.5, 114.0, 118.9, 120.2, 121.0, 124.0, 127.1, 128.0, 138.7, 142.8, 146.0, 148.4, 149.4, 160.1. MS *m/z* (%): 327 (55), 326 (M^+, 100). Anal. Elem. Calc. for $C_{19}H_{18}O_5$: C, 69.93; H, 5.56. Found: C, 69.91; H, 5.53.

3-(2′,4′-Dimethoxyphenyl)-6-methylcoumarin (75′). Yield 55%. Mp 154–155 °C. ^{1}H NMR ($CDCl_3$) δ: 2.40 (s, 3H, CH_3), 3.81 (s, 3H, OCH_3), 3.83 (s, 3H, OCH_3), 6.55–6.57 (m, 2H, H-3′, H-5′), 7.25–7.30 (m, 4H, H-5, H-6′, H-7, H-8), 7.67 (s, 1H, H-4). ^{13}C NMR ($CDCl_3$) δ: 21.0, 55.7, 56.0, 99.4, 104.8, 116.4, 117.1, 119.6, 126.1, 127.7, 131.7, 132.2, 134.1, 141.6, 151.9, 158.6, 161.2, 161.6. MS *m/z* (%): 298 (8), 297 (43), 296 (M^+, 100). Anal. Elem. Calc. for $C_{18}H_{16}O_4$: C, 72.96; H, 5.44. Found: C, 73.10; H, 5.50.

8-Methoxy-3-(m-tolyl)coumarin (76). Yield 64%. Mp 151–152 °C. ^{1}H NMR ($CDCl_3$) δ: 2.43 (s, 3H, CH_3), 4.00 (s, 3H, OCH_3), 7.07–7.15 (m, 2H, H-4′, H-6′), 7.20–7.25 (m, 2H, H-7, H-5′), 7.28 (s, 1H, H-2′), 7.35 (t, 1H, H-6, J = 7.9), 7.50 (dd, 1H, H-5, J = 7.9, 1.9), 7.79 (s, 1H, H-4). ^{13}C NMR ($CDCl_3$) δ: 21.7, 56.5, 113.4, 119.5, 120.6, 124.5, 125.9, 128.6, 128.9, 129.4, 129.8, 134.9, 138.3, 140.1, 143.3, 147.2, 160.2. MS *m/z* (%): 266 (M^+, 100). Anal. Elem. Calc. for $C_{17}H_{14}O_3$: C, 76.68;

H, 5.30. Found: C, 76.70; H, 5.27.

A solution of substituted 3-(3′,4′-dimethoxyphenyl)-6-methylcoumarin (**9**, 0.50 mmol) in acetic acid (5 mL) and acetic anhydride (5 mL), at 0 °C, was prepared. Hydriodic acid 57% (10 mL) was added dropwise. The mixture was stirred, under reflux temperature, for 3 h. The solvent was evaporated under vacuum, and the dry residue was purified by CH_3CN crystallization to give the coumarin **71**.

3-(3′,4′-Dihydroxyphenyl)-6-methylcoumarin (71). Yield: 92%. Mp 199–200 °C. ^{1}H NMR (DMSO-d_6) δ: 2.43 (s, 3H, CH_3), 6.43 (s, 1H, H-2′), 7.01 (d, 1H, H-5′, J = 7.1), 7.14 (d, 1H, H-6′, J = 7.1), 7.28–7.32 (m, 2H, H-7, H-8), 7.57 (d, 1H, H-5, J = 2.2), 7.83 (s, 1H, H-4), 10.40 (s, 2H, OH). ^{13}C NMR (DMSO-d_6) δ: 20.7, 100.1, 110.7, 111.6, 115.7, 119.4, 120.1, 127.3, 127.4, 132.1, 133.7, 138.8, 146.5, 146.8, 151.3, 161.6. MS *m/z* (%): 269 (13), 268 (M^+, 100). Anal. Calc. for $C_{16}H_{12}O_4$: C, 71.64; H, 4.51. Found: C, 71.60; H, 4.49.

A solution of 3-(2,4-dimethoxyphenyl)-6-methylcoumarin (**75′**, 1.0 mmol), NBS (1.2 mmol) and AIBN (cat.) in CCl_4 (5.0 mL) was stirred under reflux for 18 h. The resulting solution was filtered to remove succinimide. The solvent was evaporated under vacuum, and purified by flash chromatography (hexane–EtOAc, 95:5) to give the coumarin **75**.

3-(5′-Bromo-2′,4′-dimethoxyphenyl)-6-methylcoumarin (75). Yield 78%. Mp 208–209 °C. ^{1}H NMR ($CDCl_3$) δ: 2.43 (s, 3H, CH_3), 3.86 (s, 3H, OCH_3), 3.96 (s, 3H, OCH_3), 6.58 (s, 1H, H-3′), 7.21–7.32 (s, 3H, H-5, H-7, H-8), 7.54 (s, 1H, H-6′), 7.66 (s, 1H, H-4). ^{13}C NMR ($CDCl_3$) δ: 20.8, 56.2, 56.5, 96.9, 101.9, 116.2, 118.0, 119.1, 125.0, 127.6, 132.3, 134.0, 134.4, 141.8, 151.8, 157.1, 157.8, 160.4. MS *m/z* (%): 377 (21), 376 (1 0 0), 375 (25), 374 (M^+, 99). Anal. Elem. Calc. for $C_{18}H_{15}BrO_4$: C, 57.62; H, 4.03. Found: C, 57.56; H, 4.10.

4.3. Determination of MAO isoforms in vitro activity

The effects of the 3-thiophenylcoumarins on *h*MAO enzymatic activity were evaluated by a fluorimetric method following the experimental protocol previously described by us. Briefly, 50 μL of sodium phosphate buffer (0.05 M, pH 7.4) containing the test molecules (new compounds or reference inhibitors) in different concentrations and adequate amounts of recombinant *h*MAO-A or *h*MAO-B [adjusted to obtain in our experimental conditions the same reaction velocity (*h*MAO-A: 1.1 μg protein; specific activity: 150 nmol of *p*-tyramine oxidized to *p*-hydroxyphenylacetaldehyde/min/mg protein; *h*MAO-B: 7.5 μg protein; specific activity: 22 nmol of *p*-tyramine transformed/min/mg protein)] were incubated for 10 min at 37 °C in a flat-black bottom 96-well microtest plate, placed in the dark fluorimeter chamber. After this incubation period, the reaction was started by adding 50 μL of the mixture containing (final concentrations) 200 μM of the Amplex® Red reagent, 1 U/mL of horseradish peroxidase and 1 mM of *p*-tyramine. The production of H_2O_2 and, consequently, of resorufin, was quantified at 37 °C in a multidetection microplate fluorescence reader (Fluo-star Optima™, BMG LABTECH, Offenburg, Germany) based on the fluorescence generated (excitation, 545 nm, emission, 590 nm) over a 10 min period, in which the fluorescence increased linearly. Control experiments were carried out simultaneously by replacing the tested molecules with appropriate dilutions of the vehicles. In addition, the possible capacity of these molecules to modify the fluorescence generated in the reaction mixture, due to non-enzymatic inhibition (i.e. for directly reacting with Amplex® Red reagent), was determined by adding these molecules to solutions containing only the Amplex® Red reagent in sodium phosphate buffer. The specific fluorescence emission (used to obtain the final results) was calculated after subtraction of the background activity, which was determined from wells containing all components except the *h*MAO isoforms, which were replaced by sodium phosphate buffer solution.

Acknowledgements

This project was partially supported by the University of Porto (Portugal), University of Santiago de Compostela (Spain), Centro Singular de Investigación de Galicia, Spain (acreditación 2016-19, ED431G/05), Xunta de Galicia, Spain (Galician Plan of Research, Innovation and Growth 2011–2015, Plan I2C, ED481B 2014/086–0 and ED481B 2018/007) and Fundação para a Ciência e Tecnologia, Portugal (FCT, CEECIND/02423/2018). M. M. thanks to Comisión Nacional de Investigación Científica y Tecnológica (CONICYT, Chile, Fondecyt Postdoctoral Grant 3180408). The authors would like to thank Professor Lourdes Santana for her scientific support. Authors would like to thank the use of RIAIDT-USC analytical facilities.

Appendix A. Supplementary data

Supplementary data to this article can be found online at https://doi.org/10.1016/j.bioorg.2020.103964.

References

[1] D.K. Simon, C.M. Tanner, P. Brundin, Parkinson disease epidemiology, pathology, genetics, and pathophysiology, Clin. Geriatr. Med. 36 (1) (2020) 1–12.
[2] L.G. Iacovino, F. Magnani, C. Binda, The structure of monoamine oxidases: Past, present, and future, J. Neural Tranms. 125 (11) (2018) 1567–1579.
[3] G. Pagano, G. Rengo, G. Pasqualetti, G.D. Femminella, F. Monzani, N. Ferrara, M. Tagliati, Cholinesterase inhibitors for Parkinson's disease: a systematic review and meta-analysis, J. Neurol. Neuros. Psyc. 86 (2015) 767–773.
[4] I. Engelbrecht, J.P. Petzer, A. Petzer, Evaluation of selected natural compounds as dual inhibitors of catechol-O-methyltransferase and monoamine oxidase, Cent. Nerv. Syst. Agents Med. Chem. 19 (2) (2019) 133–145.
[5] A. Alonso Cánovas, R. Luquin Piudo, P. García Ruiz-Espiga, J.A. Burguera, V. Campos Arillo, A. Castro, G. Linazasoro, J. López Del Val, L. Vela, J.C. Martínez Castrillo, Dopaminergic agonists in Parkinson's disease, Neurologia. 29 (4) (2014) 230–241.
[6] Wolfgang H. Oertel, Recent advances in treating Parkinson's disease, F1000Res 6 (2017) 260, https://doi.org/10.12688/f1000research10.12688/f1000research.10100.1.
[7] E. Uliassi, F. Prati, S. Bongarzone, M.L. Bolognesi, Medicinal chemistry of hybrids for neurodegenerative diseases, Des. Hyb. Mol. Drug Develop. (2017) 259–277.
[8] A. Stefanachi, F. Leonetti, L. Pisani, M. Catto, A. Carotti, Coumarin: a natural, privileged and versatile scaffold for bioactive compounds, Molecules. 23 (2) (2018) 250–284.
[9] D. Srikrishna, C. Godugu, P.K. Dubey, A review on pharmacological properties of coumarins, Mini Rev. Med. Chem. 18 (2) (2018) 113–141.
[10] M.J. Matos, D. Viña, S. Vazquez-Rodriguez, E. Uriarte, L. Santana, Focusing on new monoamine oxidase inhibitors: differently substituted coumarins as an interesting scaffold, Curr. Top. Med. Chem. 12 (20) (2012) 2210–2239.
[11] A. Gaspar, N. Milhazes, L. Santana, E. Uriarte, F. Borges, M.J. Matos, Oxidative stress and neurodegenerative diseases: looking for a therapeutic solution inspired on benzopyran chemistry, Curr. Top. Med. Chem. 15 (5) (2015) 432–445.
[12] G.L. Delogu, M.J. Matos, Coumarins as promising scaffold for the treatment of age-related diseases - an overview of the last five years, Curr. Top. Med. Chem. 17 (29) (2017) 3173–3189.
[13] G.F. Mangiatordi, D. Alberga, L. Pisani, D. Gadaleta, D. Trisciuzzi, R. Farina, A. Carotti, G. Lattanzi, M. Catto, O. Nicolotti, A rational approach to elucidate human monoamine oxidase molecular selectivity, Eur. J. Pharm. Sci. 101 (2017) 90–99.
[14] C. Zhang, K. Yang, S. Yu, J. Su, S. Yuan, J. Han, Y. Chen, J. Gu, T. Zhou, R. Bai, Y. Xie, Design, synthesis and biological evaluation of hydroxypyridinone-coumarin hybrids as multimodal monoamine oxidase B inhibitors and iron chelates against Alzheimer's disease, Eur. J. Med. Chem. 180 (2019) 367–382.
[15] D. Tao, Y. Wang, X.Q. Bao, B.B. Yang, F. Gao, L. Wang, D. Zhang, L. Li, Discovery of coumarin Mannich base derivatives as multifunctional agents against monoamine oxidase B and neuroinflammation for the treatment of Parkinson's disease, Eur. J. Med. Chem. 173 (2019) 203–212.
[16] S. Rauhamäki, P.A. Postila, S. Niinivehmas, S. Kortet, E. Schildt, M. Pasanen, E. Manivannan, M. Ahinko, P. Koskimies, N. Nyberg, P. Huuskonen, E. Multamäki, M. Pasanen, R.O. Juvonen, H. Raunio, J. Huuskonen, O.T. Pentikäinen, Structure-activity relationship analysis of 3-phenylcoumarin-based monoamine oxidase B inhibitors, Front Chem. 6 (2018) 41.
[17] B.P. Repsold, S.F. Malan, J. Joubert, D.W. Oliver, Multi-targeted directed ligands for Alzheimer's disease: design of novel lead coumarin conjugates, SAR QSAR Environ. Res. 29 (3) (2018) 231–255.
[18] B. Mathew, G.E. Mathew, J.P. Petzer, A. Petzer, Structural Exploration of Synthetic Chromones as Selective MAO-B Inhibitors: A Mini Review, Comb. Chem. High Throughput Screen. 20 (6) (2017) 522–532.
[19] D. Secci, S. Carradori, A. Bolasco, P. Chimenti, M. Yáñez, F. Ortuso, S. Alcaro, Synthesis and selective human monoamine oxidase inhibition of 3-carbonyl, 3-acyl,

and 3-carboxyhydrazido coumarin derivatives, Eur. J. Med. Chem. 46 (10) (2011) 4846–4852.
[20] M.J. Matos, C. Terán, Y. Pérez-Castillo, E. Uriarte, L. Santana, D. Viña, Synthesis and study of a series of 3-arylcoumarins as potent and selective monoamine oxidase B inhibitors, J. Med. Chem. 54 (20) (2011) 7127–7137.
[21] M.J. Matos, S. Vilar, V. García-Morales, N.P. Tatonetti, E. Uriarte, L. Santana, D. Viña, Insights into functional and structural properties of 3-arylcoumarins as an interesting scaffold in MAO-B inhibition, ChemMedChem 9 (2014) 1488–1500.
[22] C. Fernandes, C. Martins, A. Fonseca, R. Nunes, M.J. Matos, R. Silva, J. Garrido, B. Sarmento, F. Remião, F.J. Otero-Espinar, E. Uriarte, F. Borges, PEGylated PLGA nanoparticles as a smart carrier to increase the cellular uptake of a coumarin-based monoamine oxidase B inhibitor, ACS Appl. Mater. Interfaces. 10 (46) (2018) 39557–39569.
[23] A. Fonseca, J. Reis, T. Silva, M.J. Matos, D. Bagetta, F. Ortuso, S. Alcaro, E. Uriarte, F. Borges, Coumarin versus Chromone Monoamine Oxidase B Inhibitors: Quo Vadis? J. Med. Chem. 60 (16) (2017) 7206–7212.
[24] G. Ferino, S. Vilar, M.J. Matos, E. Uriarte, E. Cadoni, Monoamine oxidase inhibitors: ten years of docking studies, Curr. Top. Med. Chem. 12 (20) (2012) 2145–2162.
[25] A. Golbraikh, A. Tropsha, Beware of q 2!, J. Mol. Graph. Model. 20 (4) (2002) 269–276.
[26] A. Golbraikh, M. Shen, Z. Xiao, Y.D. Xiao, K.H. Lee, A. Tropsha, Rational selection of training and test sets for the development of validated QSAR models, J. Comput. Aided Mol. Des. 17 (2–4) (2003) 241–253.
[27] K. Roy, I. Mitra, S. Kar, P.K. Ojha, R.N. Das, H. Kabir, Comparative studies on some metrics for external validation of QSPR models, J. Chem. Inf. Model. 52 (2) (2012) 396–408.
[28] Nicola Chirico, Paola Gramatica, Real External Predictivity of QSAR Models. Part 2. New Intercomparable Thresholds for Different Validation Criteria and the Need for Scatter Plot Inspection, J. Chem. Inf. Model. 52 (8) (2012) 2044–2058, https://doi.org/10.1021/ci300084j.
[29] C. Rucker, G. Rucker, M. Meringer, y-Randomization and its variants in QSPR/QSAR, J. Chem. Inf. Model. 47 (6) (2007) 2345–2357.
[30] K. Roy, S. Kar, P. Ambure, On a simple approach for determining applicability domain of QSAR models, Chem. Intell. Lab. Syst. 145 (2015) 22–29.
[31] M. Mellado, C.O. Salas, E. Uriarte, D. Viña, C. Jara-Gutiérrez, M.J. Matos, M. Cuellar, Design, synthesis and docking calculations of prenylated chalcones as selective monoamine oxidase B inhibitors with antioxidant activity, Chemistryselect 4 (26) (2019) 7698–7703.
[32] E. Abad, R.K. Zenn, J. Kastner, Reaction mechanism of monoamine oxidase from QM/MM calculations, J. Phys. Chem. B 117 (46) (2013) 14238–14246.
[33] M.J. Matos, F. Perez-Cruz, S. Vazquez-Rodriguez, E. Uriarte, L. Santana, F. Borges, C. Olea-Azar, Remarkable antioxidant properties of a series of hydroxy-3-arylcoumarins, Bioorg. Med. Chem. Lett. 21 (13) (2013) 3900–3906.